ADVANCED FUNCTIONAL MATERIALS
www.afm-journal.de

Integration of Mechatronic Functions on Additively Manufactured Components via Laser-Assisted Selective Metal Deposition

Tobias Vieten, Sascha Weser, Alexander Schilling, Kerstin Gläser, and André Zimmermann**

The current industrial revolution derives much of its momentum from value creation based on interconnected products and related data based services. Such products must fulfill both mechanical and electrical requirements, making them mechatronic systems. The production of such systems via additive manufacturing (AM) processes offers advantages in achievable complexity, reduction of the amount of individual components, and cost-effective as well as sustaina ble production of small quantities. In this work, a process chain is presented that allows for refining additively manufactured 3D structures made from industry-standard materials into mechatronic components by creating electrically conductive structures directly on their surfaces. The process chain is based on masking the component's surface and selectively removing the masking according to the circuit geometry using laser radiation. In a wet–chemical bath process, the surface is then exposed to palladium nuclei, the masking is fully removed and metal layers (copper/nickel/gold) are deposited by electroless plating. The procedure is developed using stereolithography as a model process for AM and transferred to four additional AM methods. In all cases, despite markedly different surface properties, good selectivity of metal deposition is observed as well as adhesion strength and conductivity comparable to industrially common injection-molded laser direct structured mechatronic interconnect devices.

1. Introduction

As additive manufacturing (AM) technologies are employed increasingly in an industrial context, it is clear that they are recognized as a means for the economical production of individualized products or small to medium series. With the "complexity for free" approach, a single additively manufactured part can be a system in itself, equipped with a multitude of mechanical functions such as hinges, sliding surfaces, fixtures, and more.[1] Starting in 1999, efforts to integrate electronic functions into parts made via additive manufacturing have been published.[2] Such 3D mechatronic systems, also called mechatronic integrated devices (MID),[3] are becoming especially relevant as an enabler for Industry 4.0 megatrends such as the Internet of Things (IoT) or Cyber-Physical Systems (CPS) and derived business models based on the economization of collected data.[4] Compared to 2D printed circuit boards (PCB), MID can have a higher degree of design freedom and integration density, which in many cases allows for further miniaturization of electronics and mechatronic systems.

Over the past 30 years, many different technologies have been used to produce additively manufactured mechatronic integrated devices (AM-MID), sometimes by themselves or paired with another AM technology but often incorporated in a more or less complex process chain. In the supporting information, we provide an overview of some published technology combinations in Table S1 (Supporting Information), itemized by the technologies for the production of the base component and the electrical structures. Typically, the electrical structures are produced with the same or another AM technology, a laser-based process or a direct-write (DW) process. DW processes, as defined by Hon et al., are those used to precisely deposit functional or structural materials in digitally defined areas on a substrate surface, unlike AM technologies, which are employed for the construction of 3D structures.[5]

The published processes usually rely on novel materials or combinations of specific fabrication methods. Additive manufacturing already risks the alienation of manufacturers when they

T. Vieten, A. Schilling, A. Zimmermann
Faculty for Engineering Design
Production Engineering and Automotive Engineering
Institute for Micro Integration (IFM)
University of Stuttgart
Allmandring 9b, 70569 Stuttgart, Germany
E-mail: tobias.vieten@hahn-schickard.de; andre.zimmermann@ifm.uni-stuttgart.de

T. Vieten, S. Weser, K. Gläser, A. Zimmermann
Hahn-Schickard
Allmandring 9 b, 70569 Stuttgart, Germany

The ORCID identification number(s) for the author(s) of this article can be found under https://doi.org/10.1002/adfm.202312833

© 2024 The Authors. Advanced Functional Materials published by Wiley-VCH GmbH. This is an open access article under the terms of the Creative Commons Attribution License, which permits use, distribution and reproduction in any medium, provided the original work is properly cited.

DOI: 10.1002/adfm.202312833

are required to replace their well-proven materials with unknown powders, filaments or resins. Further reduction of their choice of materials for the benefit of mechatronic integration hinders the acceptance of those processes. Therefore, the goal of this study is a method that enables the production of AM-MID without the need of a specialized material or relying on a single AM technology.

In the course of the preliminary considerations for the process selection for such a method, we divide the possible processes into three logical categories:

(a) The base components and the geometry of the functional structures are produced using the same AM technology in the same apparatus (e.g., fused filament fabrication with a dielectric and a conducting material)
(b) The geometry of the functional structures is created simultaneously to the base component using a different method in the same apparatus (e.g., fused filament fabrication combined with a DW technology),
(c) The base components and the functional structures are produced sequentially in a process chain.
Without exorbitant time and effort the functional structures can be integrated inside of the AM component only via methods of categories "a" and "b". However, since the intention of this work is a method for the integration of mechatronic functions in components made from more or less any AM technology and material, only category "c" seems feasible. For category a there cannot be a single method that allows for the production of AM-MID with most AM technologies on their own because the different AM technologies are very dissimilar. For a method in category b, the capability of being integrated into many different AM machines would entail an extreme amount of requirements on the method. Therefore, only category "c", the process chain, holds the possibility of a successful method, which, for reasons of practicality, limits the available section of a component to its surface. Otherwise, the product would need to go through the process chain – including cleaning steps etc. – repeatedly for the amount of layers with functional structures within.

Noteworthy candidates for functionalization processes are DW methods and laser-based methods. Laser processing holds a significant speed advantage over DW methods and the inks and pastes processed with DW methods usually require sintering at temperatures exceeding 100 °C to establish electrical conductivity. This limits the selection of base materials to those with glass transition temperatures significantly above the sintering temperature, as the residual stresses introduced into the component due to the layer-by-layer additive manufacturing process could lead to component warping, rendering it unusable. Examining existing products containing MID components, one can find more examples of laser-based processes than DW methods. Consequently, a higher industry acceptance can be assumed for a laser-based process, which is the goal here.

In the intersection of DW and laser-based processes lies a group of methods using laser-based selective direct metal patterning (LSDMP), one of which is nano ink-based laser sintering developed by Grigoropoulos' group at UC Berkeley.[6] The methods use the nanoparticle inks or metal precursors developed for, e.g., inkjet printing by selectively,[7,8] fully[9,10] or partially (according to a regular[11] or random[12] pattern) coating the substrate surface and then applying laser radiation to selectively sinter particles in the area relevant for the electrical circuits. Because nanoparticles have a lower melting temperature compared to bulk material and the laser can heat up a small region in a short time, the heat-affected zone on the substrate can be kept to a minimum. Depending on the method, sub-micron feature sizes can be achieved. Although the process was originally developed for gold nanoparticles, other groups transferred it to copper ,[11,12,13] silver,[9,14,15] and nickel.[10,16] The laser-based selective direct metal patterning methods were developed for the production of 2D systems based on foils, sheets or wafers, yet, some published versions of the method might be adapted for the functionalization of 3D components. By jetting or spray coating the nanoparticle inks onto the surface of 3D components and quickly drying them, a layer of sinterable material might be achievable, if the surface is smooth and closed such as is the case on material jetted components. For irregular or even porous surfaces of, e.g., laser-sintered components this seems hardly achievable, which is why LSDMP methods probably do not qualify for functionalizing an arbitrary AM component. In combination with LSDMP a similar process was also developed for semiconducting materials via the selective growth of ZnO nanowires.[17,18] The semiconducting structures are used for UV light sensing. Here too, a process transfer on additively manufactured 3D components does not seem feasible due to the poor surface quality of the components.

An existing commercial method for producing AM-MID based on laser processing is the product ProtoPaint LDS by LPKF Laser & Electronics SE from Garbsen, Germany.[19,20] It consists of a coating containing laser direct structuring (LDS) activators[3] that can be directly applied to a component to generate conductive structures on the component through laser structuring and electroless plating. However, this coating is only suitable for prototype production, as the metal layer along with the coating often delaminates from the substrate material when the component is subjected to stress. Particularly, the system's durability under thermal cycling stress is significantly reduced due to the coating in the layer structure. This is especially the case with unfilled substrate materials, due to the mismatch in the coefficient of thermal expansion between metal an polymer.[21] Moreover, such coatings are difficult to apply on AM components due to their roughness and porosity. For example, the process described by Mager et al., which relies on an LDS-capable coating, only works after a two-stage component pre-treatment involving primer and filler materials.[22] Currently, LPKF no longer offers ProtoPaint LDS for purchase. For the method described here can be inferred, that, for the sake of reliability, the current-carrying structures should be directly applied to the surface without introducing an additional permanent intermediate layer.

There are literature-known methods for selective electroless plating on non-specific polymeric 3D base components. Some of these methods are subtractive or semi-additive MID technologies based on conventional photolithography, similar to PCB technology, where an injection molded component is first fully electrolessly plated with copper, then coated with a photoresist which is exposed through a 3D mask and developed, and the excess

© 2024 The Authors. Advanced Functional Materials published by Wiley-VCH GmbH

copper etched away.[23] If necessary, the copper is reinforced by electroplating. Marques-Hueso et al. developed a similar process specifically for Polyetherimide (PEI) in the form of foils and flat fused filament fabricated components.[24] Due to disadvantages such as the necessity of fabricating and using individual 3D exposure masks, these methods are not suitable for combination with agile digital processes such as additive manufacturing. Other methods are based on laser-induced selective surface modification, which, compared to the non-laser-treated surface, results in different adsorption behavior of the corresponding catalyst suspensions for the subsequent electroless plating processes. After immersing the laser-structured base components in the catalyst suspension, a washing process removes the catalyst from the original surfaces. Due to the specific topology in the laser-structured areas, the catalyst can only be washed off much more slowly, leading to the desired selective behavior of chemically-reductive metal deposition. Such process chains have been developed for injection molded components by Zhang for thermoplastic materials[25] and by Kordass for thermosetting materials.[26] For foils, Ren et al.[27] have presented their work. Both Zhang and Kordass conclude that the selective seeding with catalytic particles primarily relies on diffusion processes into and out of the microporous structures of the laser-treated surfaces (ideally a foam or sponge-like structure). The diffusion speed and depth differ between structured and unstructured areas due to varying topology. Unprocessed injection-molded components initially possess a very smooth and dense surface, which is disrupted by the laser beam. For instance, in Zhang's work, the roughness of surfaces before laser structuring is given at approximately $S_a = 0.6$ µm, and after laser treatment, it increases up to $S_a = 5.7$ µm. This corresponds to an increase of about a factor of 10. Additively manufactured components usually exhibit a significantly rough surface due to the manufacturing process, especially powder-based methods that generate surfaces with a structure formed by firmly adhering powder particles. Achieving a further increase in roughness by an order of magnitude through laser processing does not seem promising. In the publicly funded study LasMet3D, the selective seeding of additively manufactured components through surface roughening by laser irradiation was investigated.[28] Components built via digital light processing (DLP) were used in the study, which already have relatively smooth and closed surfaces. However, a satisfactory outcome in the form of selective metal deposition was not achieved. When considering other works from the literature that have pursued similar approaches, the aforementioned issue of a poorly selective metallization becomes apparent there as well. Ratautas et al. describe the SSAIL method, where fused filament fabrication (FFF) components made from PC/ABS are laser treated, seeded with silver nitrate, and metalized through electroless plating. Although only a small portion of the sample surface is displayed, a comparison with also investigated injection-molded samples reveals that the FFF components exhibit more pronounced excess copper deposition.[46] In summary, it can be observed that the differences in surface characteristics achieved through laser processing on various examples of additively manufactured components are not sufficient for selective metal deposition. Consequently, the conclusion is drawn that such a process is not readily suitable for the production of AM-MID based on a random AM method. For a stable process, ideally, the activator solution should never come into contact with surfaces where no metal deposition is intended. One approach is to protect the surface of the component with temporary masking before it is exposed to the activator solution. When the mask is selectively removed by laser irradiation, it enables selective seeding of the component surface. Following seeding, the rest of the masking material can be removed.

1.1. Process Description

In the current work, the SANCHO method is proposed: Integration of mechatronic functions by **S**elective metal deposition on **A**dditively ma**N**ufactured components using wet–chemical processes and laser-based surface m**O**dification (acronym originally derived from the german nomenclature).

The process chain begins with the fabrication of the base component using any additive manufacturing method. The component is coated with a masking material using a dipping process. The masking is partially removed via laser radiation, exposing the areas of the component's surface that will later depict the circuitry. By immersing the component in a Pd-based activator solution, catalytic seeds are deposited on the surface and, where possible, penetrate it through diffusion processes. The mask and the seeds on its surface are removed from the component using suitable solvents to avoid unwanted metal deposition and negative effects on the usability of the AM-MID. The selectively seeded component then undergoes further electroless plating processes. These processes involve the catalytic action of the remaining seeds on the component's surface, causing a reduction of metal salts in the solution, thereby enabling the desired metal deposition on the component's surface. The specific metals used depend on the intended product; common choices for MID and circuit boards involve depositing layers composed of copper as the electric conductor, nickel as a diffusion barrier, and gold as an oxidation barrier.

2. Results and Discussion

The two primary requirements of the SANCHO method are, first, the generation of functional and reliably electrically conductive structures on the component surface, and second, the applicability of the process to a wide range of different additive manufacturing processes and materials. These two demands were examined by first developing the processes for adding conductive structures on components made with a model AM technology and a model material and then applying the method to additional AM technologies and materials in a condensed manner.

2.1. Masking

Figure 1 illustrates the results of the masking experiments. The upper row shows DLP-components, the second row SLS-components, both with increasing amounts of PGMEA from left to right. The components were immersed in the masking material up to the dashed line. In the top row, it can be observed that even with the highest examined dilution, a dense masking layer can still be applied to DLP components. Due to the rough and

© 2024 The Authors. Advanced Functional Materials published by Wiley-VCH GmbH

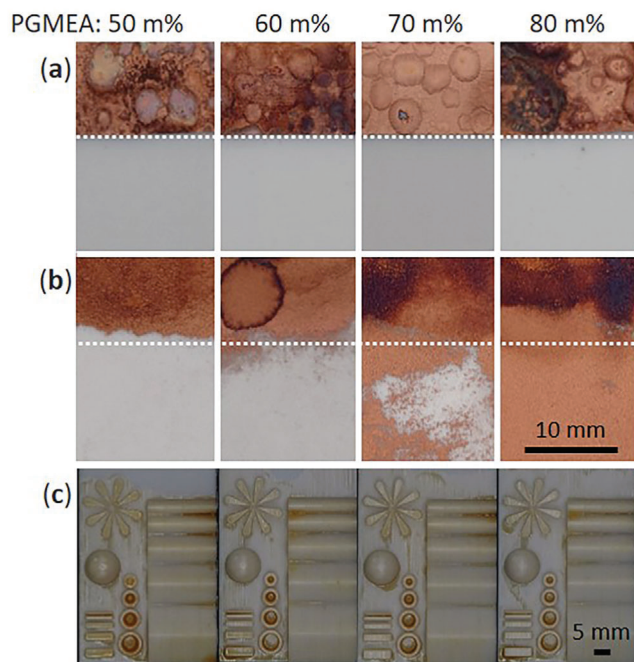

Figure 1. Study of resist dilution: a) DLP-components dipped to the dashed line; b) SLS-components dipped to the dashed line; c) DLP-components fully immersed.

porous surface of the SLS components, a dilution is only possible up to a maximum of 60, preferably 50 m%, before the mask becomes ineffective.

Figure 1c shows four complex components coated with the previously mentioned dilution levels. Particularly in the round troughs lacquer accumulates at each dilution level. This could likely be prevented by spinning off the excess lacquer. However, in the region of varying opening angles and edge radii, a more even coating is achieved with a higher solvent content in the lacquer, especially in the upper area (opening angle 50°). Due to geometric features, the layer thickness of the coating will not always be equally thick. Up to a certain level this is not critical, as the laser is powerful enough to ablate the mask material and some of the component itself in one run. If the mask is too thick in certain areas this can also be met with design rules for the geometry of the AM component such as minimum values for edge radii or hole and slot sizes. An influence of layer thickness variations on the width of the ablated structures was not identified, so it should be in the same order of magnitude as the waviness of the edge geometry caused by the metal deposition.

A commercial negative resist originally developed for lithography processes was employed here. This choice was made because such resists can be readily dissolved and are already used in electronics manufacturing so they are compatible with following assembly processes. However, it would be beneficial to develop a masking material with tailored properties. For instance, components of the resist that are unnecessary for the SANCHO process, such as those related to photosensitivity, could be omitted, making the product cheaper and more eco-friendly. The coating process parameters need to be reconsidered for each base material and AM technology. In some cases, plasma pretreatment might be beneficial to render poorly wettable materials accessible for masking.

2.2. Laser Parameter Screening (Copper Layer Thickness and Adhesion Strength)

Figure 2a shows the results of the laser study on a masked DLP component made from PLASTCure Rigid 10500 after copper deposition. The component was coated with negative photoresist, laser processed, activated, and metalized to assess the effectiveness of the individual parameter sets.

Fields with insufficient metal deposition or burning, especially if they affect neighboring fields, were omitted from further investigations. The remaining parameter sets were used for investigations into copper layer thickness and adhesion strength.

The measured values of the copper layer thickness on the examined component (Figure 2b) vary significantly, ranging between about 5 and 10 µm. With minor deviations, a qualitative correlation with the irradiation dose can be observed here, where higher values correspond to a thicker copper layer. The irradiation dose H_I describes the average amount of energy irradiated per unit area through multiple exposures during processing. Both Ratautas et al.[29] and Ninz[30] found out, that for a parameter analogous to the irradiation dose a qualitative correlation to the characteristics of the metallization exists, although it may not allow for analytically predictable conclusions. In this case, it was calculated according to Equation (1), with the average laser power P, the scanning speed v, laser focus diameter d_s, the pulse pitch s_P, and the line pitch s_L (which are set equal, here).

$$H_I = \frac{P}{v \cdot d_s} \cdot \frac{d_s}{s_L} = \frac{P}{v \cdot s_P} \tag{1}$$

The calculated values of H_I for the laser parameter study are given in Figure 2c.

In principle, for low resistance and high current-carrying capacity, parameters resulting in a thicker layer are preferable. Therefore, parameters #3, #4, #18, #19, and #34 are of special interest (indicated by dark blue coloring). These surfaces were all laser processed with a low feed rate (1 m s^{-1}) and an irradiation dose of at least 2 J mm^{-2}.

Due to the varying roughness of the component surface after laser processing, different levels of adhesion strength can be expected for each set of laser processing parameters. Therefore, four test pads were created for each parameter set to measure the adhesion strength. The average values are given in Figure 2d. The highest adhesion strength values were measured in fields #18 (19.55±0.66 N mm^{-2}) and #19 (21.46 ± 1.98 N mm^{-2}). These fields also exhibited high copper layer thickness measurements. The lowest value was measured in field #42 (10.29 ± 0.41 N mm^{-2}). When comparing the results to published adhesion strength values within the realm of MID and AM-MID technology (**Table 1**), the values are comparable even to LDS PEEK MID. Parameter sets on the lower end still surpass those of LDS LCP MID, a common material for injection-molded circuit carriers. In the search for literature data, attention was paid that across all sources the HBPM with a pin diameter of 900 µm was used to ensure comparability.

© 2024 The Authors. Advanced Functional Materials published by Wiley-VCH GmbH

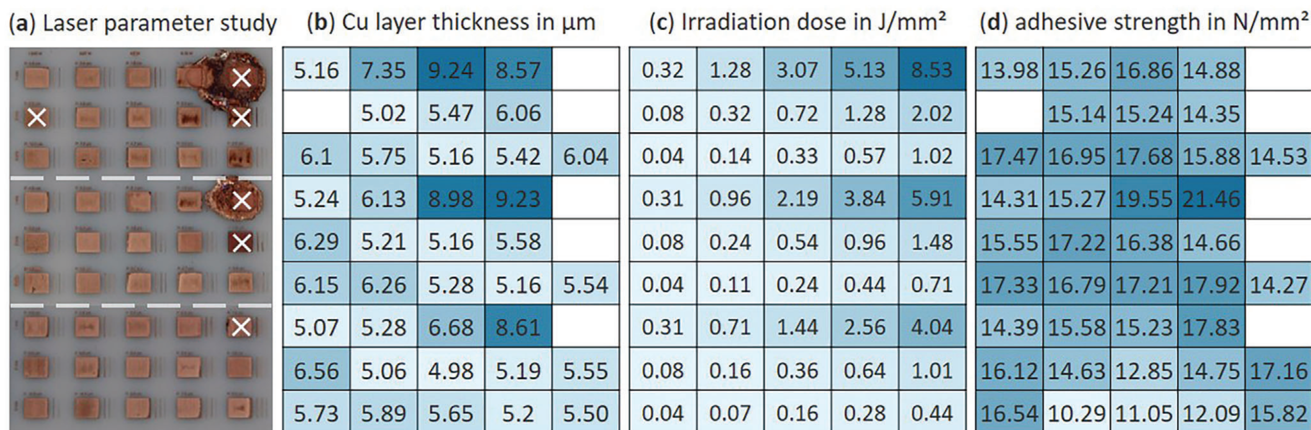

(b) Cu layer thickness in µm

5.16	7.35	9.24	8.57	
	5.02	5.47	6.06	
6.1	5.75	5.16	5.42	6.04
5.24	6.13	8.98	9.23	
6.29	5.21	5.16	5.58	
6.15	6.26	5.28	5.16	5.54
5.07	5.28	6.68	8.61	
6.56	5.06	4.98	5.19	5.55
5.73	5.89	5.65	5.2	5.50

(c) Irradiation dose in J/mm²

0.32	1.28	3.07	5.13	8.53
0.08	0.32	0.72	1.28	2.02
0.04	0.14	0.33	0.57	1.02
0.31	0.96	2.19	3.84	5.91
0.08	0.24	0.54	0.96	1.48
0.04	0.11	0.24	0.44	0.71
0.31	0.71	1.44	2.56	4.04
0.08	0.16	0.36	0.64	1.01
0.04	0.07	0.16	0.28	0.44

(d) adhesive strength in N/mm²

13.98	15.26	16.86	14.88	
	15.14	15.24	14.35	
17.47	16.95	17.68	15.88	14.53
14.31	15.27	19.55	21.46	
15.55	17.22	16.38	14.66	
17.33	16.79	17.21	17.92	14.27
14.39	15.58	15.23	17.83	
16.12	14.63	12.85	14.75	17.16
16.54	10.29	11.05	12.09	15.82

Figure 2. Results of the laser parameter study: a) photo of a machined component with burnt parameter sets marked by a white x, b) copper layer thickness after electroless plating (average of four measurements), c) calculated irradiation dose, d) adhesive strength of the copper layer (average of four measurements).

The roughness of the surface produced by the laser ablation probably does not only affects the adhesion strength between metal and polymer but may also affect the electrical properties of the circuit itself. As proposed, the roughened surface should correspond with more trapped activator particles, which leads to faster metal deposition and therefore thicker conductive layers. This corresponds to the shown data on copper layer thickness and irradiation dose. Additionally, a higher roughness also produces a larger surface area. Together, these effects should produce a larger cross section for the metal circuit locally and thereby increased conductivity. Yet, globally, the resistance of an irregular shaped conductive line is strongly influenced by its smallest cross-sectional area. Statistically a higher roughness might produce stronger "bottlenecks" and thereby reduce the conductivity of the whole circuit. This effect should be weaker the wider a line is designed as statistical variations in the cross-section are less likely to have a significant impact.

2.3. Selectivity and Resistivity

For a DLP component masked with negative resist and processed using parameter set #18, the short electrical test layout (ETL) is depicted in **Figure 3**a, and the long ETL in Figure 3b. Overall, a good selectivity of metal deposition can be observed. Although overplating is present to some extent, it mostly appears in the form of thin strands. Upon examination under a stereomicroscope, it can be observed that they are often elevated from the surface at one end, likely originating from metalized dust particles. Despite the presence of overplating, no short circuit current was detected during the measurements. However, all four investigated structures consistently exhibited conductivity, which speaks to good deposition behavior despite their narrow width of 100 µm.

The laser used for the development of the SANCHO process has a focus diameter of 23 µm. When ablating mask material in

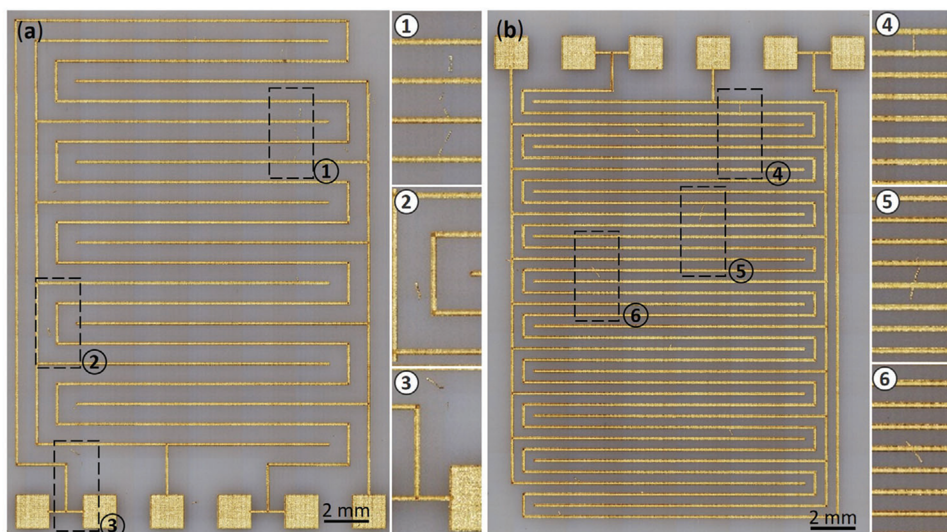

Figure 3. Photos of a DLP component processed with the SANCHO method: a) short ETL; b) long ETL.

© 2024 The Authors. Advanced Functional Materials published by Wiley-VCH GmbH

a single line this is also almost exactly the width of the deposited copper trace. This means that to some extent the minimum trace width can be reduced by using a more focused laser beam. Yet, this is only true for smooth and closed surfaces such as on DLP components. The true limiting factor will be the surface topology of the AM component. Especially with powder-based processes, due to the irregularity and the open pores of the polymer surface, the width of the electrical circuits should be at least in the range of 100 to 300 µm to reliably produce conductive traces.

In order to investigate the selectivity of metal deposition on 3D parts, DLP components in the form of four-sided truncated pyramids were built. Resist mixed with 70% PGMEA was utilized for masking. Overall, selective metal deposition is also evident here (**Figure 4**).

For the laser parameter set #18, a resistance of ≈0.023 Ω per millimeter of conductor length is obtained. Although the width of the conductor is only 100 µm, this result is approximately in line with the findings of Amend et al.,[34] who deposited copper on SLA components using the ADDIMID process and reported a resistance of 1 Ohm for a 500 µm wide and 15 mm long trace, which translates to a length-specific resistance of 0.067 Ω mm^{-1}. Balzereit et al.[35] deposited copper on SLS components and measured the resistance between two probe points spaced 2 mm apart. The trace width is greater than the length, and therefore can be considered to be infinite. They reported a resistance of 0.3 Ω, which corresponds to a length-specific resistance of 0.15 Ω mm^{-1}.

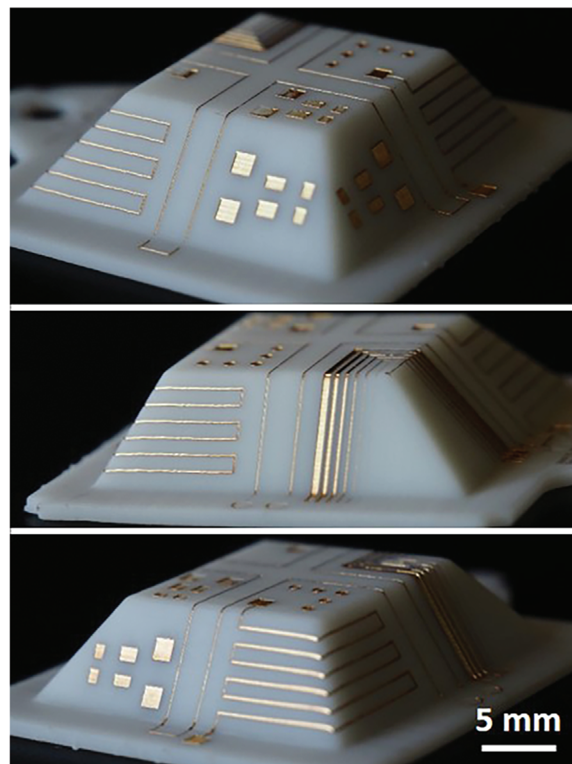

Figure 4. Photos of a 3D component (DLP).

Table 1. Comparison of different MID production methods regarding adhesion strength of chemically deposited copper on polymer. All references were measured via HBPM (pin diameter 900 µm). Production method noted on base polymer: [1]LDS MID, [2]SSAIL MID, [3]SSAIL AM-MID, [4]SIPA MID, [5]SANCHO AM-MID.

Polymer	Name, Manufacturer	Adhesion Strength	Reference
LCP[1]	TECACOMP LCP LDS black 4107, Ensinger	8.6 N mm^{-2}	[31]
PEEK[1]	TECACOMP PEEK LDS black 3980, Ensinger	20 N mm^{-2}	[31]
PPA[1]	Vestamid HTplus TGP 3586, Evonik	19 N mm^{-2}	[32]
PPA[1]	Vestamid HTplus TGP 3586, Evonik	17.9 N mm^{-2}	[33]
LCP[1]	Vectra LCP E840iLDS, Celanese	8.9 N mm^{-2}	[33]
PA6[2]	Ultramid B2S, BASF	7.2 N mm^{-2}	[29]
PPA[2]	HTNF8200 NC010, DUPONT	8 N mm^{-2}	[29]
PC/ABS[2]	LNP THERMOCOMP Compound NX10302, SABIC	8.3 N mm^{-2}	[29]
PMMA[2]	140 HF, SABIC	3.8 N mm^{-2}	[29]
PEEK[2]	450FE20, VIKTREX	12 N mm^{-2}	[29]
ABS[3]	PC/ABS Filament, Stratasys	5.4 N mm^{-2}	[29]
Epoxy[4]	Epoxidur EP 3581 T-1, Raschig	12.7 N mm^{-2}	[26]
Epoxy[5]	PLASTCure Rigid 10500, Prodways Materials	21.5 N mm^{-2}	–

2.4. Transfer to Other AM Technologies

2.4.1. Stereolithography

Due to the relatively smooth surfaces, the SLA components were masked with the more diluted negative resist (70 m% PGMEA). From the laser study, parameter set #28 was chosen. The adhesion strength measurements yielded an average value of 4.74 ± 0.28 N mmΩ^2, which is relatively low. Nevertheless, the ETL structures are conductive and free from short circuits, with a length-specific resistance of ≈0.077 Ω mm^{-1} (**Table 2**). The images in **Figure 5**a,e show good, selective metal deposition. The structures are free from interruptions, and there is virtually no overplating on the components.

2.4.2. PolyJet

Due to the smooth surfaces, the PolyJet components were masked with the more diluted negative resist (70 m% PGMEA). However, on the 3D components, this led to a full-surface metal

© 2024 The Authors. Advanced Functional Materials published by Wiley-VCH GmbH

Table 2. Results of the adhesion (average of four measurements and standard deviation) and resistance measurements as well as length-specific resistance.

AM method	Laser parameter set	Adhesion	Resistance[length]	Length specific resistance
DLP	#18 (4.6 W, 1 m s^{-1}, 469.6 kHz)	21.5 ± 2 N mm^{-2}	4.7 Ω (200 mm)	0.024 Ω mm^{-1}
			6.6 Ω (300 mm)	0.022 Ω mm^{-1}
SLA	#28 (4.6 W, 3 m s^{-1}, 469.6 kHz)	4.7 ± 0.3 N mm^{-2}	15.5 Ω (200 mm)	0.078 Ω mm^{-1}
			22.9 Ω (300 mm)	0.076 Ω mm^{-1}
PolyJet	#37 (3.07 W, 2 m s^{-1}, 208.7 kHz)	9.7 ± 1.2 N mm^{-2}	12.1 Ω (200 mm)	0.061 Ω mm^{-1}
			18.0 Ω (300 mm)	0.060 Ω mm^{-1}
SLS	#27 (3.07 W, 3 m s^{-1}, 313.1 kHz)	13.7 ± 5.4 N mm^{-2}	3.5 Ω (200 mm)	0.018 Ω mm^{-1}
			– Ω (300 mm)	– Ω mm^{-1}
MJF	#22 (3.07 W, 2 m s^{-1}, 313.1 kHz)	12.8 ± 2.4 N mm^{-2}	5.8 Ω (200 mm)	0.029 Ω mm^{-1}
			9.1 Ω (300 mm)	0.30 Ω mm^{-1}

deposition on the flanks. Therefore, these components were rebuilt and double-masked with the less diluted negative resist (50 m% PGMEA). From the laser study, parameter set #37 was selected. Adhesion strength measurements yielded an acceptable average of 9.67 ± 1.24 N mmΩ^2. The deposited meander comb structures are all conductive and free from short circuits, with a length-specific resistance of ≈0.06 Ω mm^{-1} (Table 2). The images in Figure 5b,f show good selective metal deposition. The structures are free from interruptions, and there is virtually no overplating on the components.

2.4.3. Selective Laser Sintering

Due to the surface structure, the SLS components were masked with the less diluted negative resist (50 m% PGMEA). From the laser study, parameter set and #27 was selected. Adhesion strength measurements yielded an average of 13.67 ± 5.43 N mm^{-2} (Table 2). However, there is overplating present and the structures are not conductive, so they evidently have interruptions. As mentioned in Section 4.1.4., parts manufactured using the SLS process are often subjected to vibratory finishing or sandblasting due to their surface properties. Therefore, additionally, vibratory finished components were examined. These were also masked with the less diluted negative resist (50 m% PGMEA). In laser processing, the same parameter set was used. This resulted in a conductive path (only short ETL) with a length-specific resistance of about 0.018 Ω mmΩ^1 (Table 2). Furthermore, the selectivity of the metal deposition on the 3D components was significantly improved (Figure 5c,g). It has not yet been investigated, but it is very well possible that SLS components without additional finishing could be processed using undiluted resist.

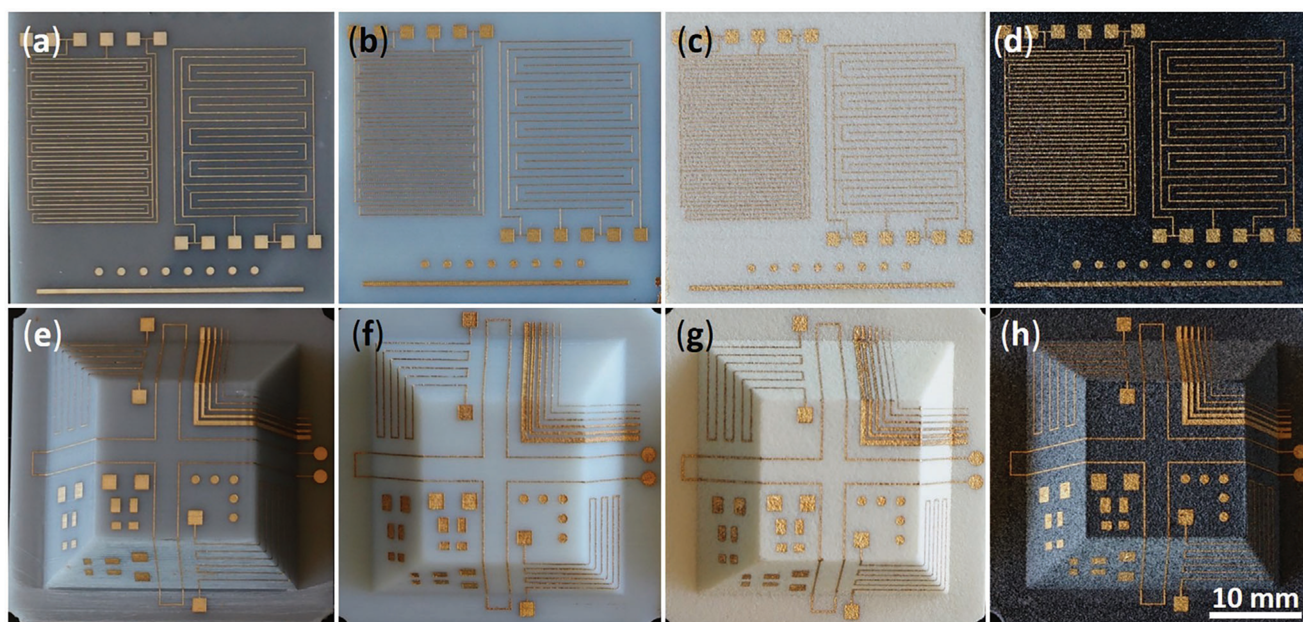

Figure 5. Photos of 2D and 3D components processed with the SANCHO method: a) SLA, b) PolyJet, c) SLS, d) MJF, e) SLA, f) PolyJet, g) SLS, h) MJF.

 © 2024 The Authors. Advanced Functional Materials published by Wiley-VCH GmbH

2.4.4. Multi Jet Fusion

The MJF components were masked with the less diluted negative resist (50 m% PGMEA). From the laser study, parameter set #22 was selected. The adhesive strength measurements yielded an acceptable average value of 12.84 ± 2.37 N mm^{-2}. The plated ETL structures are conductive and free of short circuits, with a length-specific resistance of about $0.03\ \Omega\ mm\Omega^{1}$ (Table 2). As can be seen in Figure 5d,h, there is no overplating on either the 2D or the 3D component. Therefore, compared to the SLS components, the mask seems to conform to the surface more uniformly due to its somewhat denser structure.

3. Conclusion

The SANCHO method presented in this work serves the purpose of constructing mechatronic assemblies based on additively manufactured components. It is the first process chain that is presented as a method for the direct application of conductive structures onto the surface of a component made from standard materials using different (or possibly any) additive manufacturing techniques.

Through preliminary considerations and investigations, a process chain was developed, including the application of a temporary mask on the component, selective removal of the mask through laser ablation, and a series of wet–chemical bath processes for applying a catalyst, final removal of the mask, and electroless plating of a metal layer. The method was established using Digital Light Processing as a model additive manufacturing technique and a model material in the form of a glass-filled photopolymer. The properties of the current-carrying structures were characterized in terms of adhesion strength and conductivity. Additionally, the transferability of the process was demonstrated on four other additive manufacturing processes and materials, namely stereolithography, Stratasys PolyJet, selective laser sintering, and HP Multi Jet Fusion. These processes were selected due to their significantly differing surface characteristics, and successful metal deposition with good selectivity was demonstrated on components from all five additive manufacturing processes. Adhesion strengths and conductivities comparable to industrially typical injection-molded circuit carriers were confirmed.

For future development of the SANCHO process, process parameters should be established for additional additive manufacturing processes, for example fused filament fabrication, which is a very common AM technology. Detailed exploration was carried out here only for the model process and model material. A full process development should be undertaken for more AM technologies and the reliability of mechatronic assemblies on different base materials should be investigated. This would enable predictions about the service life, which is essential for industry acceptance of the SANCHO method beyond prototyping.

4. Experimental Section

Additive Manufacturing of Polymer Parts—Digital Light Processing (Rigid 10500): For processing glass-filled thermosetting plastics, a material class most alike the base material of commonly used PCBs, either dispensing methods (from the material extrusion class) or vat photopolymerization (VPP) processes are suitable. Dispensing methods have the advantage of being able to process materials with higher viscosity, allowing for a higher filler content and thus a lower coefficient of thermal expansion (CTE). However, they operate at a slow pace, especially when resolution and surface quality are emphasized. VPP processes work relatively fast and are therefore preferable for industrial applications. For VPP processes, commercially available materials based on acrylates, epoxides, and/or polyurethanes that were already filled with glass beads exist. These materials were often designed for specific machine types and a narrow wavelength range. For process development in this work, the VPP method of digital light processing was used with the photopolymer PLASTCure Rigid 10500 (Prodways Materials, Friedberg, Germany), which consisted of a mixture of acrylates and epoxides and, according to measurements, was filled with ≈60 wt.% SiO_2 powder. The material was processed on a ProMaker L5000 digital light processing system (Prodways, Montigny-le-Bretonneux, France), which was based on top-down VPP with a wavelength of 365 nm. Very similar materials from other providers include Somos PerForm (Stratasys) or Accura HPC (3D Systems).

Additive Manufacturing of Polymer Parts—Stereolithography (Accura Xtreme): Stereolithography (SLA) is the oldest additive manufacturing process and, like DLP, belongs to the vat photopolymerization class of AM methods. Accordingly, the material used, Accura Xtreme (3D Systems, Rock Hill, USA), is thermosetting, yet, unlike PLASTCure Rigid 10500, it is unfilled. It was processed on a SLA Viper system (3D Systems, Rock Hill, USA). The energy input for material crosslinking was provided through ultraviolet laser irradiation. Components build using stereolithography typically exhibited a relatively smooth surface. An exception were surfaces that rely on support structures during the build process. They featured a pitted texture due to the removal of supports. These surfaces were often smoothed via grinding or blasting processes, resulting in a corresponding surface texture. To achieve a consistent appearance, manufacturing service providers frequently apply post-processing evenly on all surfaces.

Additive Manufacturing of Polymer Parts—Stratasys PolyJet (VeroWhite Plus): The PolyJet process by Stratasys belongs to the AM category of material jetting. Utilizing InkJet technology, a photopolymer was applied in the form of very fine droplets onto a build platform and cured by a UV lamp. The used material, VeroWhite Plus (Stratasys Ltd., Rehovot, Israel), a thermoset, was colored white, though it remains translucent, and was processed on an Objet350 system (Stratasys Ltd., Rehovot, Israel). The small volumes of the droplets, in the range of a few picoliters, allow for very high resolutions in all directions and produced among the smoothest surfaces achievable in the AM field. However, this also prevented the incorporation of fillers, limiting the thermomechanical properties of the materials. A second print head can deposit wax as support material, enabling smooth and areal support for overhanging areas, thus facilitating the construction of very uniform surfaces here as well. Post-processing of surfaces was usually unnecessary once the wax was thermally removed from the surface.

Additive Manufacturing of Polymer Parts—Selective Laser Sintering (PA12): Selective Laser Sintering (SLS) is a process within the powder bed fusion category of additive manufacturing. The input of energy to sinter the powder particles is achieved through laser irradiation. The utilized PA 2200 Performance 1.0 powder (EOS GmbH, Krailling, Germany) was based on the material polyamide 12 and was processed on a Formiga P100 system (EOS GmbH, Krailling, Germany). The SLS process is a widely used method in the polymer AM domain. As the parts were automatically supported by the un-sintered powder during the build in the powder bed, components could be freely positioned in the build area, allowing for high machine utilization. Consequently, the step of support removal was eliminated. Nevertheless, the surface of the components varied depending on whether they were oriented more upward in the build area (smoother) or downward (irregular/rough). Generally, however, all surfaces were formed by partially sintered powder particles and were correspondingly rough and open-porous. SLS components were often post-processed through processes like vibratory finishing, bead blasting, or sandblasting to smoothen or compact the surface.

© 2024 The Authors. Advanced Functional Materials published by Wiley-VCH GmbH

Additive Manufacturing of Polymer Parts—HP Multi Jet Fusion (PA12): The Multi Jet Fusion (MJF) process by HP (Palo Alto, USA), similar to SLS, is also a method within the powder bed fusion category of additive manufacturing. However, the energy input for sintering the powder particles in this case occurs uniformly through a heating lamp. The selectivity of sintering was achieved through the deposition of two inks using InkJet technology. The first ink ("fusing agent") was deposited in the areas that will form the final component. The heat radiation was absorbed from the lamp and reacts with the powder, causing the particles to fuse together. The second ink ("detailing agent") was deposited in the areas of the powder bed that should not sinter. This ink dissipated the energy it receives. The high resolution of the InkJet process allowed for greater detail accuracy compared to SLS processes. The used HP 3D High Reusability PA 12 powder (HP) was based on the material polyamide 12 and appears gray to the eye. In reality, it consists of a mixture of white and black colored particles, which can make a difference in the following laser processing step. It was processed on a HP Jet Fusion 4200 System. The statements from the section about SLS regarding support of components by the powder bed, surface characteristics, and post-processing also apply to MJF. However, the surfaces tend to be somewhat denser in MJF.

Masking with Lacquer: To suppress metal deposition on untreated surfaces, the AM components are coated with a protective mask. Since additive manufacturing enables the production of complex components, the coating process must be suited to apply a thin layer of material even on hard-to-reach surfaces. Methods such as spin coating or continuous processes (e.g., curtain coating or doctor blade coating) were ill-suited for 3D applications. Spray processes, which allow for uniform and controlled material application, quickly become complex or reach their limits when dealing with intricate component geometries. In this regard, dip-coating processes had an advantage due to their simplicity. A variety of lacquers was used in microsystems technology, with the most widely known probably being solder mask, which gave printed circuit boards (PCB) their characteristic green color. For temporary masking, the removability of the lacquer was an important property. In silicon and PCB technology, photosensitive resist masks were used in lithographic processes. They were designed to be completely removable using solvents to avoid interfering with subsequent processes. These resists were typically available in various versions for application via spin coating or spraying, with the spraying variant containing a higher solvent content to reduce viscosity. The investigated resist AR-N 4400–10 (Allresist GmbH, Strausberg, Germany) was obtained as a thick resist for spin coating and diluted with the solvent propylene glycol methyl ether acetate (PGMEA) to achieve a viscosity suitable for the dip-coating process. To investigate proper dilution levels, DLP and SLS components were partially dipped in the resist (50, 60, 70, and 80 m% PGMEA) and dried at 80 °C for 40 min. Besides DLP components made from PLASTCure Rigid 10500, which had relatively smooth surfaces, SLS components made from PA12 powder were chosen due to their rough and porous surfaces. Subsequently, the components were treated with an activator solution, the resist was removed, and metal was deposited. The addition of the solvent aims to create a thin, uniform masking layer during the dipping process. On complex 3D components, undiluted resist tends to form reservoirs and beads in crevices and corners, which, beyond a certain thickness ratio, will not be fully removed during laser processing. To investigate this behavior, DLP test components with a complex 3D geometry were built and dip-coated. The component geometry is shown in **Figure 6**a. It has features that are prone to accumulate masking material, e.g., in holes or via capillary action.

Selective Laser Ablation of the Mask Layer: The masking is selectively removed with a laser to create a discrete circuit layout. At the same time the component surface was modified by the laser to create a rough and rugged structure. This surface modification initially allowed better embedding of activator particles in the surface structure, leading to reduced particle washout during rinsing processes, resulting in increased metal deposition. Additionally, this enhanced the adhesion of the metal layer to the component, as the metal fills undercuts in the polymer and mechanically interlocks with it. The laser system used in this study is a Nd:YVO4 laser with a wavelength of 532 nm, a focus diameter of 23 µm, a pulse duration of 10 ps and a frequency of 200 to 20 000 kHz. 45 parameter sets were

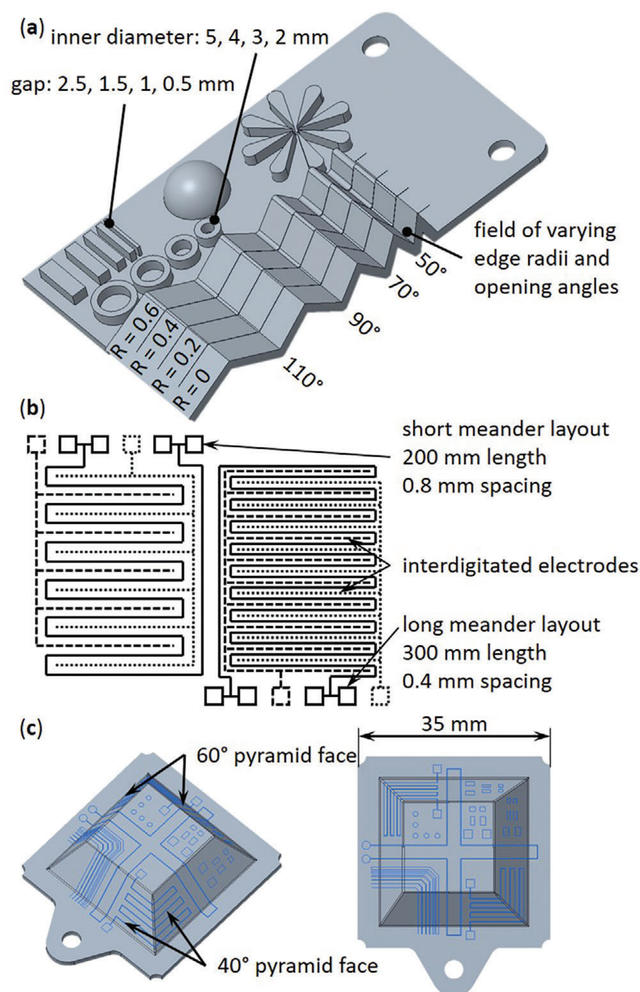

Figure 6. Test layouts. a) electrical layout with meandering conductor and interdigitated electrodes; b) truncated pyramid with different side angles; c) component with complex surface geometry for resist dipping tests.

investigated, using a variation of scan speed, averaged laser power, and pulse frequency. The pulse pitch was a result of the scan speed and the pulse frequency while the line pitch was set to be equal to the pulse pitch. The parameter sets were arranged on the test components in fields from left to right and top to bottom. This arrangement is also represented in Table S2 (Supporting Information), where the individual parameter sets are given.

Wet Chemical Processing Steps: After laser processing, the process chain only consists of wet chemical immersion and rinsing steps. The rinsing steps were carried out reproducibly with an automated program, aiming to prevent the carryover of chemicals between the individual baths. In the sequence of baths, the component was first immersed in an activator to seed the laser-processed surface with a catalyst. The activator also deposited on the surface of the mask. A subsequent acceleration step enhanced the catalytic properties of the activator particles. Subsequently, the masking was removed by immersing the component in an alkaline solution, and the catalytically active seeds should now be present only on the laser-processed surfaces. Next, the component was sequentially immersed in baths for electroless plating of metals, typically copper (Cu), nickel (Ni), and gold (Au). The individual process steps were explained in the following sections.

Wet Chemical Processing Steps—Catalytic Activation: Palladium-based activators exist as commercial products and are utilized in various

© 2024 The Authors. Advanced Functional Materials published by Wiley-VCH GmbH

processes. In PCB technology, palladium is used to activate VIAs (vertical interconnect access) in multilayer PCBs for electroless chemical copper deposition. Palladium also plays a significant role in plating on plastics processes for surface pretreatment before wet–chemical metal deposition.[36] The mechanisms of palladium-activated copper deposition are discussed extensively in the literature, e.g. by Kanani.[37] For the SANCHO process, the commercial product UDIQUE 879 W Activation (MacDermid Enthone, Langenfeld, Germany) was used, which is a colloidal activator for plating on plastics processes.[38] The accompanying accelerator is the product UDIQUE 8810 Accelerator (MacDermid Enthone).[39] The products were used according to manufacturer instructions.

Wet Chemical Processing Steps—Mask Removal: As previously indicated the photosensitive resist can be removed from the component surface using alkaline solutions. In this case aqueous potassium hydroxide solution (KOH) was used in a concentration of 56 g KOH per liter of water (≙ 1 mol L^{-1}, pH 14) at 50 °C. This allows for a complete removal of the masking within about 3 min without influencing the activator particles.

Wet Chemical Processing Steps—Metal Deposition: Common commercial copper electrolytes are alkaline and contain formaldehyde (HCHO) as a reducing agent, as well as stabilizers and complexing agents that prevent the precipitation of copper hydroxide. In an alkaline medium, formaldehyde decomposes, providing electrons for the reduction of copper salt.[37]

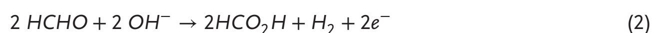

$$2\ HCHO + 2\ OH^{-} \rightarrow 2HCO_2H + H_2 + 2e^{-} \tag{2}$$

$$Cu^{2+} + 2e^{-} \rightarrow Cu \tag{3}$$

Copper, due to its low resistivity, forms the main part of the conductive layer. However, it is susceptible to oxidation in moist air, where the resulting copper(I) oxide and copper(II) oxide, due to their poorer conductivity and solderability, can impair the overall system's reliability.[40] A thin gold layer can initially protect the copper from oxidation, but with warming due to a manufacturing process or current flow, the gold's crystal lattice becomes increasingly permeable to the smaller copper atoms due to their larger atomic diameter. Hence, the copper atoms diffuse through the thin gold layer and are exposed to the atmosphere again, after which they oxidize which increases the electrical resistance at the surface, leading to greater heating and accelerated diffusion.[41] This escalating cycle continues until the system fails. Therefore, a nickel layer is deposited between the copper and gold layers, effectively acting as a diffusion barrier due to nickel's smaller atomic radii. This layer sequence, copper/nickel/gold, was widely used, well-tested, and described in various sources in both PCB and MID technology.[3,42,43]

For copper deposition, the commercial electrolyte Circuposit 3350–1 (DuPont de Nemours Inc., Wilmington, USA) was used.[44] The process duration for activated components was 90 min. For nickel deposition, the commercial electrolyte Durni-Coat (RIAG Oberflächentechnik AG, Wängi, Switzerland) was used.[45] The dwell time in the bath was 15 min, resulting in a layer thickness of ≈5 µm. For the immersion gold process, the commercial product Auroblex 20 (Blendl Gmbh, Metzingen, Germany) was used.[46] The dwell time was 10 min⸜, resulting in a layer thickness of ≈0.1 µm. All products were used and applied according to manufacturer instructions.

Examination: For the investigations, components were masked with lacquer, laser-processed using the parameter sets presented in Table 2S and metallized, in order to derive suitable process parameters based on the layer thickness and adhesion strength of the metal layer. After selecting two sets of parameters, additional structures were created with these parameter sets to assess the selectivity of metal deposition and measure electrical conductivity.

Examination—Layer Thickness Measurements via X-Ray Fluorescence Spectroscopy: To measure the thickness of deposited metal layers, there are several different approaches. On the one hand there are manual measurement techniques like light microscopy based on a cross-section or the differential profile measurement before and after metal deposition. On the other hand there were established methods like the X-ray fluorescence analysis (XRF). The advantage of XRF is its ability to be automated and performed at a large number of measurement points, providing user-independent measurement values. In XRF, primary radiation in the form of high-energy X-rays was directed onto the test object. The atoms of the sample were ionized by the primary radiation, removing electrons close to the nucleus. However, this state was unstable and an electron from a higher shell fills the gap and emits fluorescence radiation. The energy of this secondary radiation was characteristic for the specific material. Via the location and intensity of peaks in the registered spectrum the types and amounts of materials can be inferred. In this study, the thickness of copper layers was measured for every laser parameter set after 90 min of deposition using X-ray fluorescence analysis (Fischerscope XDV-µ, Helmut Fischer GmbH, Sindelfingen) on four different areas.

Examination—Adhesion Strength Measurements via Hot Bump Pull Method: The adhesion strength was measured using the hot bump pull method (HBPM). This measurement method was developed by Nordson Dage, Aylesbury, UK, and conducted here using the Nordson DAGE 4000Plus measurement system. In this method, a copper pin with a diameter of 900 µm was inserted into a heated measurement module and clamped in place. The copper pin had a semi-spherical rounded end on its face. Corresponding to the pin diameter, metal structures with a diameter of 900 µm were deposited on the surface of the sample. After applying solder paste to the measurement pad, the copper pin was positioned on the pad and the measurement module heats the pin according to a temperature-time profile tailored to the solder and substrate material. The solder melted, forming a mechanical connection between the copper pin and the pad. The measurement module then pulled the copper pin upward while measuring the tensile force exerted on the layer system using a force sensor. The known area of the measurement pad allows the breaking force to be converted into mechanical stress values. The method was also described and investigated by Goth et al.[32] Due to the varying roughness of the component surface after laser processing, different levels of adhesion strength are expected for each set of laser processing parameters. Therefore, four test pads were generated for each parameter set, and their adhesion strengths were measured and averaged.

Examination—Electrical Resistivity Testing: The electrical resistance R of a real conductor is determined by geometric and material-specific factors. It depends on the specific resistance ρ_{sp} (or the electrical conductivity κ) of the material, as well as the cross-sectional area A and the length l of the conductor, according to Equation (4).

$$R = \rho_{sp} \cdot \frac{l}{A} = \frac{1}{\kappa} \cdot \frac{l}{A}. \tag{4}$$

The specific resistance (also known as specific electrical resistance or resistivity) is a temperature-dependent material constant and the reciprocal of the electrical conductivity κ. Compared at room temperature, copper has the third highest electrical conductivity after graphene and silver. Yet, the specific conductivity of chemically deposited copper on MID reaches only about 60 % of that of pure copper.[3,47] The thickness of electrically conductive structures is limited by the chemical deposition process and varies due to surface structure. Therefore, the resistance of the produced structures can largely only be adjusted through their width. Here, the resistivity is specified for a fixed conductor width of 0.1 mm and divided by it's length. The resistance was measured on the copper layer using the four-point measuring method (Keysight 34410A) on meandering conductors (200 and 300 mm long) shown in Figure 6b, before the deposition of nickel and gold. The deposition time in the copper bath was 90 min.

Examination—Selectivity of the Metal Deposition: For the design of mechatronic systems, the selectivity of the metal plating process is an important criterion. The quantity and geometry of metal structures on non-laser-processed surfaces (overplating) determine the spacing at which circuits must run to minimize the risk of short circuits. Similarly, the formation of gaps in the metal layer on laser-processed surfaces affects the minimum structure size with which a conductive connection can be reliably established, depending on the size and shape of these gaps. The selectivity of the metal plating process thus impacts the miniaturization potential of the SANCHO method. To assess the selectivity of metal deposition, structures were created following the electrical test layouts (ETL) shown in Figure 6b. These layouts include a meandering path with

 © 2024 The Authors. Advanced Functional Materials published by Wiley-VCH GmbH

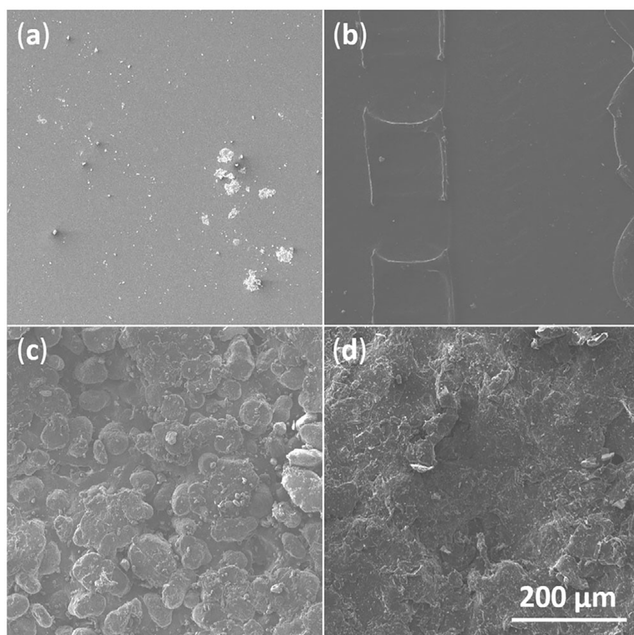

Figure 7. SEM images of components from the studied AM technologies. a) Stereolithography; b) PolyJet; c) Selective Laser Sintering; d) HP Multi Jet Fusion.

two interdigitated electrodes. By applying an electrical potential and measuring the resulting current with a multimeter, short circuits (current between the meander and either of the two interdigitated electrodes) and breaks (no current on meander) can be detected with these layouts. Two of these layouts with differing spacing and length were utilized. The longer conductor is 300 mm in length with a spacing of 0.4 mm between meander and interdigitated electrodes, while the shorter is 200 mm in length with a spacing of 0.8 mm. The width of all conductive paths is 0.1 mm. To investigate the selectivity on 3D components, the geometry shown in Figure 6c was built and processed. It consists of a square truncated pyramid with two 40° and two 60° faces.

Transfer to Other AM Technologies: To demonstrate the applicability of the SANCHO method across different AM technologies and materials, investigations were conducted on four additional processes. These investigations aimed to showcase the fundamental feasibility and do not constitute a complete process development. The emphasis for the AM technologies was placed on a diverse range of surface characteristics. On the material side, thermosetting polymers in the form of photopolymers and thermoplastics in powder form were utilized. The materials were not selected based on their properties concerning mechatronic component construction, but represent common materials for each respective process. The individual processes and materials were elaborated in Section 2.1. **Figure 7** provides an initial insight into the surface structure of components for the examined processes through SEM images. Subfigure (a) shows a stereolithography component, which is a thermosetting plastic part formed from a stationary liquid. Subfigure (b) displays a Stratasys PolyJet component, constructed drop by drop using a thermosetting plastic. Both exhibit a smooth surface. Subfigure (c) presents a laser-sintered component, produced from a thermoplastic powder. Subfigure (d) depicts an HP Multi Jet Fusion component, also created from thermoplastic powder. The latter exhibits a more closed and distinct surface structure.

To limit the effort for the overall investigations, the individual processes were examined in less detail compared to Digital Light Processing. Masking was applied using negative resist with two different dilutions (50 or 70 m% PGMEA) based on the surface structure. A laser parameter study was conducted for each material. One set of parameters was chosen through visual examination using a stereomicroscope and 2D and 3D components were built as presented in Figure 6. The wet–chemical processes were executed with the same parameters as before. The selectivity of metal deposition was assessed using the ETL, and length-specific conductivity was determined. Additionally, eight adhesion strength measurements were performed on every material using the HBPM.

Supporting Information

Supporting Information is available from the Wiley Online Library or from the author.

Acknowledgements

Preliminary experiments for this study were conducted in the final stage of the IGF promotion plan No. 19555 N. The IGF promotion plan No. 19555 N of the Research Community for Quality (FQS), August-Schanz-Straße 21A, 60433 Frankfurt/Main was funded by the AiF within the program for sponsorship by Industrial Joint Research (IGF) of the German Federal Ministry of Economic Affairs and Energy based on enactment of the German Parliament. The authors thank CIRP GmbH and 3D-Labs GmbH for providing the stereolithography, PolyJet, selective laser sintering, and HP Multi Jet Fusion components.

Open access funding enabled and organized by Projekt DEAL.

Conflict of Interest

The authors declare no conflict of interest.

Data Availability Statement

The data that support the findings of this study are available from the corresponding author upon reasonable request.

Keywords

3D printed electronics, additive manufacturing, electrical functionalization, mechatronic integrated devices, structural electronics, selective electroless plating

Received: October 17, 2023
Revised: February 9, 2024
Published online: March 5, 2024

[1] M. Fera, R. Macchiaroli, F. Fruggiero, A. Lambiase, *Int J Adv Manuf Technol* **2018**, *95*, 673.
[2] P. D. Calvert, H. B. Denham, T. A. Anderson, in *Sensory Phenomena and Measurement Instrumentation for Smart Structures and Materials*, SPIE, Bellingham, WA **1999**, pp.128.
[3] J. Franke, *Räumliche elektronische Baugruppen (3D-MID): Werkstoffe, Herstellung, Montage und Anwendungen für spritzgegossene Schaltungsträger*, Carl Hanser Verlag, Munich, **2013**.
[4] M. R. Binelli, R. van Dommelen, Y. Nagel, J. Kim, R. I. Haque, F. B. Coulter, G. Siqueira, A. R. Studart, D. Briand, *Sci. Rep.* **2023**, *13*, 1962.
[5] K. Hon, L. Li, I. Hutchings, *CIRP Ann.* **2008**, *57*, 601.
[6] J. Chung, S. Ko, N. R. Bieri, C. P. Grigoropoulos, D. Poulikakos, *Appl. Phys. Lett.* **2004**, *84*, 801.

© 2024 The Authors. Advanced Functional Materials published by Wiley-VCH GmbH

[7] S. H. Ko, H. Pan, C. P. Grigoropoulos, C. K. Luscombe, J. M. J. Fréchet, D. Poulikakos, *Nanotechnol* **2007**, *18*, 345202.
[8] S. H. Ko, H. Pan, D. Lee, C. P. Grigoropoulos, H. K. Park, *Jpn. J. Appl. Phys.* **2010**, *49*, 05EC03.
[9] Y. Son, J. Yeo, H. Moon, T. W. Lim, S. Hong, K. H. Nam, S. Yoo, C. P. Grigoropoulos, D.-Y. Yang, S. H. Ko, *Adv. Mater.* **2011**, *23*, 3176.
[10] J. Shin, B. Jeong, J. Kim, V. B. Nam, Y. Yoon, J. Jung, S. Hong, H. Lee, H. Eom, J. Yeo, J. Choi, D. Lee, S. H. Ko, *Adv. Mater.* **2020**, *32*, 1905527.
[11] J. Kwon, H. Cho, Y. D. Suh, J. Lee, H. Lee, J. Jung, D. Kim, D. Lee, S. Hong, S. H. Ko, *Adv. Mater. Technol.* **2017**, *2*, 1600222.
[12] Y. D. Suh, J. Kwon, J. Lee, H. Lee, S. Jeong, D. Kim, H. Cho, J. Yeo, S. H. Ko, *Adv. Electron. Mater.* **2016**, *2*, 1600277.
[13] B. Kang, S. Han, J. Kim, S. Ko, M. Yang, *J. Phys. Chem. C* **2011**, *115*, 23664.
[14] H. Lee, S. Hong, J. Kwon, Y. D. Suh, J. Lee, H. Moon, J. Yeo, S. H. Ko, *J. Mater. Chem. A* **2015**, *3*, 8339.
[15] Y. Son, J. Yeo, C. W. Ha, J. Lee, S. Hong, K. H. Nam, D.-Y. Yang, S. H. Ko, *Thermochim. Acta* **2012**, *542*, 52.
[16] V. B. Nam, J. Shin, Y. Yoon, T. T. Giang, J. Kwon, Y. D. Suh, J. Yeo, S. Hong, S. H. Ko, D. Lee, *Adv. Funct. Mater.* **2019**, *29*, 1806895.
[17] S. Hong, J. Yeo, W. Manorotkul, H. W. Kang, J. Lee, S. Han, Y. Rho, Y. D. Suh, H. J. Sung, S. H. Ko, *Nanoscale* **2013**, *5*, 3698.
[18] J. Kwon, S. Hong, H. Lee, J. Yeo, S. S. Lee, S. H. Ko, *Nanoscale Res. Lett.* **2013**, *8*, 489.
[19] W. John, in *Proceedings of 9th Int. Congress Molded Interconnect Devices MID 2010*, Fuerth, Künzelsau, Germany **2010**.
[20] C. Goth, L. Tröger, *Prototyping für 3D-MID*HARTING Mitronics, Germany **2019**.
[21] H. Müller, T. Meißner, T. Grözinger, T. Vieten, M. Soltani, W. Eberhardt, A. Zimmermann, *presented at 10. Innovationsforum Smarte Technologien & Systeme*, Donaueschingen, March, **2018**.
[22] T. Mager, C. Jürgenhake, R. Dumitrescu, *In 13th Int. Congress Molded Interconnect Devices (MID)*, IEEE, Piscataway, NJ **2018**, pp.1.
[23] S. Klein, *Polymer Engineering 2* (Eds.: P. E. Helmut Schüle), Springer Vieweg, Berlin, Heidelberg, **2020**.
[24] J. Marques-Hueso, T. D. Jones, D. E. Watson, A. Ryspayeva, M. N. Esfahani, M. P. Shuttleworth, R. A. Harris, R. W. Kay, M. P. Desmulliez, *Adv. Funct. Mater.* **2018**, *28*, 1704451.
[25] Y. Zhang, H. N. Hansen, A. De Grave, P. T. Tang, J. S. Nielsen, *Int J Adv Manuf Technol* **2011**, *55*, 573.
[26] T. Kordass, *PhD Thesis*, FAU University Press, Erlangen, **2021**.
[27] J. Ren, D. Li, Y. Zhang, W. Yang, H. Nie, Y. Liu, *ACS Appl. Electron. Mater.* **2022**, *4*, 2191.
[28] S. Weser, B. Freisinger, *Werkzeuglose Fertigung von funktionalisierten 3D-Kunststoffbauteilen durch die Kombination von generativen Verfahren und laserbasierter selektiver Metallisierung (LasMet3D)* Hahn-Schickard-Gesellschaft für angewandte Forschung e.V., https://www.hahn-schickard.de/projekt-detail/lasmet3d, November, **2020**.
[29] K. Ratautas, A. Jagminien, I. Stankevicien, M. Sadauskas, E. Norkus, G. Raciukaitis, *Results Phys* **2020**, *16*, 102943.
[30] P. Ninz, *PhD Thesis*, University of Stuttgart, Shaker Verlag, Düren, **2021**.
[31] E. Hirt, K. Ruzicka, in *,2018 7th Electronic System-Integration Technology Conf. (ESTC)*, IEEE, Piscataway, NJ **2018**, p. 1.
[32] C. Goth, T. Kuhn, G. Gion, J. Franke, in *11th Int. Congress Molded Interconnect Devices – Scientific Proceedings*, Trans Tech Publications Ltd, xx xx **2014**, pp. 115.
[33] AiF IGF project report, *Charakterisierung und praxisnahe Methoden zur Prüfung von Leiterbahnen auf LDS-MID als Metall/Kunststoff-Verbundsysteme (LDS-MIDCHAMP)*, AiF, Erlangen, **2015**.
[34] P. Amend, C. Goth, J. Franke, T. Frick, M. Schmidt, in *Proc. of the 10th Int. Congress Molded Interconnect Devices*, 3D-MID e.V. Fuerth, Germany **2012**.
[35] S. Balzereit, F. Proes, V. Altstädt, C. Emmelmann, *Addit. Manuf.* **2018**, *23*, 347.
[36] R. Suchentrunk, *Kunststoff-Metallisierung (Schriftenreihe Galvanotechnik und Oberflächenbehandlung)*, 3rd ed., Leuze Verlag, Bad Saulgau **2000**.
[37] N. Kanani, *Kupferschichten*, Leuze Verlag, Bad Saulgau **2000**.
[38] *Product datasheet Udique 879 W Activation, Version 2.0.*, MacDermid Enthone GmbH, Langenfeld, Germany **2016**.
[39] *Product datasheet Udique 8810 Accelerator, Version 2.0.*, MacDermid Enthone GmbH, Langenfeld, Germany **2016**.
[40] E. Salahinejad, R. Eslami-Farsani, L. Tayebi, *Eng. Fail. Anal.* **2017**, *79*, 538.
[41] L. B. H., *Gold Bull.* **1975**, *8*, 52.
[42] J. Heber, H. Großmann, in *Elektrische Kontakte, Werkstoffe und Anwendungen: Grundlagen, Technologien, Prüfverfahren* (Ed.: E. Vinaricky), Springer, Berlin, Heidelberg, **2016**, p. 343.
[43] W. Eberhardt, H. Kück, S. Weser, *Elektronik Sonderausgabe Räumliche elektronische Baugruppen* **2011**, 24.
[44] *Product datasheed CIRCUPOSIT 3350–1 Electroless Copper, Version 0*, DuPont de Nemours Inc., Delaware, United States **2013**.
[45] *Instructions for use DURNI-COAT® electroless plating nickel bath on a hypophosphite basis, Version 2*, AMI Doduko GmbH, Pforzheim, Germany, **2008**.
[46] *Technical datasheet AUROBLEX 20 electroless gold bath, Version 1.1.*, Blendl GmbH Plating Products, Metzingen, Germany, **2017**.
[47] J. Friedrich, *PhD Thesis*, Friedrich-Alexander-Univerisity, Fürth, **2006**.
[48] G. Liu, C. Wang, Z. Jia, K. Wang, *J. Micromech. Microeng.* **2021**, *31*, 065005.

© 2024 The Authors. Advanced Functional Materials published by Wiley-VCH GmbH